Hue University Journal of Science: Natural Science
Vol. 129, No. 1B, 15–23, 2020

pISSN 1859-1388
eISSN 2615-9678

FABRICATION OF CdS/Au/TiO_2 SANDWICH NANOFIBERS FOR ENHANCED PHOTOELECTROCHEMICAL WATER-SPLITTING EFFICIENCY

Van Nghia Nguyen[1,2*], Manh Son Nguyen[2], Minh Thuy Doan[1]

[1] Department of Physics and Materials Science, Faculty of Natural Sciences, Quy Nhon University, 170 An Duong Vuong St., QuyNhon City, Vietnam
[2] Faculty of Physics, University of Sciences, Hue University, 77 Nguyen Hue St., Hue, Vietnam

* Correspondence to Van Nghia Nguyen <nguyenvannghia@qnu.edu.vn>
(*Received: 03 August 2019; Accepted: 18 March 2020*)

Abstract. The sandwich-structured CdS/Au/TiO_2 nanofibers (NFs) act as a photoanode in the photoelectrochemical cell (PEC) for hydrogen generation by splitting water. The gold nanoparticles sandwiched between the TiO_2 nanofibers and the CdS quantum dots (QDs) layers play an important role in enhancing the solar-to-chemical-energy conversion efficiency. The structure and morphology of the materials were characterized by using field-emission scanning electron microscopy (FE–SEM), transmission electron microscopy (TEM) and X-ray diffraction (XRD). The surface plasmon resonance (SPR) of the Au nanoparticles was investigated by using ultraviolet-visible (UV–Vis) diffuse reflectance spectroscopy. The PEC properties of the photoanode were measured on a three-electrode electrochemical analyzer. The obtained photoconversion efficiency of the CdS/Au/TiO_2 NFs is 4.1% under simulated-sunlight illumination with a 150 W xenon lamp. Working photoelectrode stability was tested, and the mechanism of the enhanced PEC performance was discussed.

Keywords: electrospinning, water splitting, TiO_2 nanofibers, sandwich-structured, PEC

1 Introduction

Hydrogen is widely considered as the fuel of the future because it is environmentally friendly. Among the methods of producing hydrogen, water splitting in a photoelectrochemical cell (PEC) is one of the promising ways. Among the semiconductors used for the field photo-electrochemical, TiO_2 was selected for the present investigation because it represents an appropriate choice in terms of either stability to corrosion and photocorrosion or low cost, high availability, and low toxicity [1]. In recent decades, one-dimensional (1D) nanostructured materials have become one of the hottest research fields because it facilitates charge transport and reduces the recombination of electron–hole pairs by providing a direct conduction pathway for the photo-generated electrons [2]. Numerous methods have been used for the synthesis of TiO_2 nanofibers [3-6]. Among them, electrospinning has attracted much attention because it provides a cost-effective, versatile, simple and continuous process.

However, due to its large bandgap (~3.0 eV for rutile and ~3.2 eV for anatase), TiO_2 is only active in the ultraviolet (UV) region, which contributes less than 5% of the total energy of the solar spectrum. The broad visible light absorption of TiO_2, which is about 45% of the solar spectrum, is one of the prerequisites for enhancing the solar energy conversion efficiency of TiO_2 [7]. Recently, various methods have been used to expand the absorption of wide-bandgap metal oxide

semiconductors to visible light. Nonmetal and metal doping is the most commonly used methods [2, 8], but these ways could only reduce electron–hole separation. Wide-bandgap metal-oxide semiconductors can be combined with a narrow-bandgap semiconductor to form a heterostructure that was also a solution. For example, semiconductor quantum dots (QDs) are used as photo-sensitizers because of their high ability to absorb light and control the absorption spectrum throughparticle size [9]. However, the surface trap states in QDs – metal oxide heterostructures and the subsequent charge accumulation at the surface slow down the transfer of excited electrons and holes, increasing the charge recombination rate and consuming the photogenerated charge carriers [10]. Alternatively, the incorporation of noble metals, especially Au, canbe employed to improve the visible light absorption of metaloxide semiconductors due to their surface plasmon resonance (SPR) properties [11, 12]. Nevertheless, the design of metallic plasmonic nanoparticle decorated hierarchical nanostructures with desirable stability and high efficiency in PEC water splitting is still the main challenge.

In this work, sandwich-structured CdS/Au/TiO_2 nanofibers fabricated on an indium–tin oxide (ITO) substrate act as the photoanode in the PEC for solar hydrogen generation. Herein, the gold nanoparticles sandwiched between the TiO_2 nanofibers and the CdS QDs layers play an important role in enhancing the solar-to-hydrogen conversion efficiency. The results show that the achieved photocurrent density for the CdS/Au/TiO_2 electrodes was significantly higher than that for bare Au/TiO_2 nanofibers and CdS/TiO_2 electrodes.

2 Experimental

2.1 Materials

All chemicals were purchased and used without further purification: poly(vinylpyrrolidone) (PVP) (wt. 360,000, Sigma–Aldrich Co., Ltd.), ethanol (C_2H_5OH, ≥99.8%), acetic acid (CH_3CO_2H, ≥99%), titanium tetraisopropoxide [$Ti(OiPr)_4$; 97%, Sigma–Aldrich Co., Ltd.], cadmium nitrate tetrahydrate ($(Cd(NO_3)_2{\cdot}4H_2O$), 98%, Aldrich Chemical Company, Inc.), thioacetamide (C_2H_5NS, 98%, Alfa Aesar Co., Ltd.), chloroauric acid trihydrate ($HAuCl_4$, Sigma–Aldrich Co., Ltd.), sodium sulfidepentahydrate ($Na_2S{\cdot}5H_2O$, 98%, DaeJung Chemical and Metals Co., Ltd.), sodium sulfite (Na_2SO_3, ≥98%, Sigma–Aldrich Co., Ltd), sodium sulfate (Na_2SO_4, ≥98%, Sigma–Aldrich Co., Ltd.), and distilled water (18.4 MΩ/cm).

2.2 Preparation of TiO_2NFs on ITO substrate

The TiO_2 NFs were fabricated by using the electrospinning method. First, 0.2 g of PVP was dissolved in 4 mL of ethanol for 2 h. Then, 3 mL of $Ti(OiPr)_4$ and 2 mL of acetic acid were added to the above solution and stirred for 1 h at room temperature to obtain the sufficient viscosity required for electrospinning. In the electrospinning process, the precursor was transferred into a 5-mL syringe attached to the syringe pump and fed into the metal needle. The precursor solution was then electrospun under a high DC voltage of 10 kV, applied across a distance of 12 cm toward the grounded collector. The solution was continuously injected with a syringe pump at a rate of 0.04 mL/h. The ITO conducting substrates (1 × 2 cm), a part of which (1 × 1 cm) was fixed by using tape, were placed on a grounded collector for the accumulation of NFs. After a collecting time of 20 minutes, the electrodes were dried in air for 5 h to allow the hydrolysis of $Ti(OiPr)_4$. Later, the

pISSN 1859-1388
eISSN 2615-9678

$Ti(OiPr)_4$/PVP composite nanofibers were oxidized for 3 h at 500 °C with a heating rate of 2 °C/min in air to remove the PVP and form the TiO_2 NFs on the ITO substrate.

2.3 Decorationof Au nanoparticles on TiO_2 NFs

A photo-reduction method [13] was used to deposit Au nanoparticles on the surface of TiO_2 NFs. Chloroauric acid trihydrate was dissolved in a mixture of water and ethanol solvent (volume ratio 1:3) to form an $HAuCl_4$ solution of 5 mM concentration. One millilitre of this solution and 0.02 g PVP were dispersed in 50 mL of ethanol in a Pyrex Petri dish to prepare the Au^{3+} precursor. Then, the TiO_2 NFs on the ITO substrate were immersed in the Petri dish, followed by irradiation with a 20 W UV lamp for 15 minutes to reduce Au^{3+} to Au^0. The PVP prevents the size development of Au clusters on the nanofibers. The irradiation time was optimized for photoconversion efficiency. After irradiation, the electrodes were dried at 60 °C in air. Finally, they were calcined in air at 450 °C for 1 h to remove PVP.

2.4 Preparation of CdS/Au/TiO_2 sandwich structure

The Au/TiO_2 NFs were decorated with CdS layers by using the dip-coating method. The CdS nanoparticles directly grew on the Au/TiO_2 NFs surface by soaking the electrodes in an aqueous solution of 10 mM $Cd(NO_3)_2{\cdot}4H_2O$ as a source of Cd^{2+} and 10 mM C_2H_5NS as a source of S^{2-} at 80 °C for 1 h, followed by rinsing with deionized water and natural drying.

2.5 Characterization

The morphology of the fabricated structures was examined by using field-emission scanning electron microscopy (FE–SEM; Hitachi S4800), transmission electron microscopy (TEM; JEOL JEM-2100F). The distribution of samples was measured on a FE–SEM machine equipped with an energy-dispersive X-ray spectrometer (EDX). The structures and optical property of the samples were analysed via X-ray diffraction (XRD, Siemen D5005) with Cu Kα radiation and the Ni filter and a UV–vis spectrophotometer (Carry 3000).

2.6 Photoelectrochemical measurement

The PEC properties were measured on a three-electrode electrochemical analyzer (Potentiostat/ Galvanostat Model DY2300), with the fabricated nanostructure films formed on ITO as aworking electrode, a platinum (Pt) wire as a counter electrode, and Ag/AgCl in saturated KCl as a reference electrode. The electrolyte used for the TiO_2 and Au/TiO_2 structures consists of 0.5 M Na_2SO_4, whereas that for CdS/Au/TiO_2 (or CdS/TiO_2) structures consists of 0.25 M Na_2S and 0.35 M Na_2SO_3 as sacrificial agents. A simulated sunlight source 150 W Xe lamp (Gloria – X150A) with an intensity of 100 mW·cm^{-2} coupled with an AM 1.5G filter was also employed to evaluate the efficiency of the photoanodes. All the measurements were performed with the front-side illumination of the photoanodes. The potential was swept linearly at a scan rate of 10 mV·s^{-1}. The illuminated area of the working electrode exposed to the electrolyte was fixed at 1 cm^2 by using nonconductive epoxy resin. The conversion efficiency was calculated according to equation (1)

$$\eta(\%) = J_P \cdot (E_{rev} - E_{app}) \cdot 100/I_0 \quad (1)$$

where J_P is the photocurrent density (mA·cm^{-2}); I_0 is the irradiance intensity of the incident light (100 mW/cm^2); E_{rev} is the standard state-reversible potential (1.23V *vs*. NHE); $E_{app} = E_{meas} - E_{aoc}$ is the applied potential, where E_{meas} is the electrode potential of the working electrode at which the photocurrent was measured under illumination and E_{aoc} is the electrode potential of the same working electrode under open-circuit conditions [14].

3 Results and discussion

Figure 1 shows the XRD patterns of TiO_2 NFs, Au/TiO_2 NFs and CdS/Au/TiO_2 NFs structures.

The XRD data collected in the 2θ range of 20–60° with a step of 0.02° show the existence of anatase TiO_2 structure (at 2θ = 25.23°, 37.86°, and 47.89°) (JCPDS file no. 84-1286). There are also two peaks at 38.1° and 44.5°, corresponding to the diffraction on the (111) and (200) planes (JCPDS file no. 65–8601) of Au face-centred cubic structure with respect to Au/TiO_2 NFs, CdS/Au/TiO_2 NFs. In addition, two diffraction peaks at 25.1° and 28.5°, corresponding to the (100) and (101) crystal planes are indicative of a hexagonal CdS structure (JCPDS file no. 80-0006). The broad peak observed for CdS suggests that the CdS grown on the surface of the TiO_2 NFs takes particulate forms. The crystallite size of the CdS coated on the TiO_2 fibers is about 15 nm, calculated from the Scherrer formula.

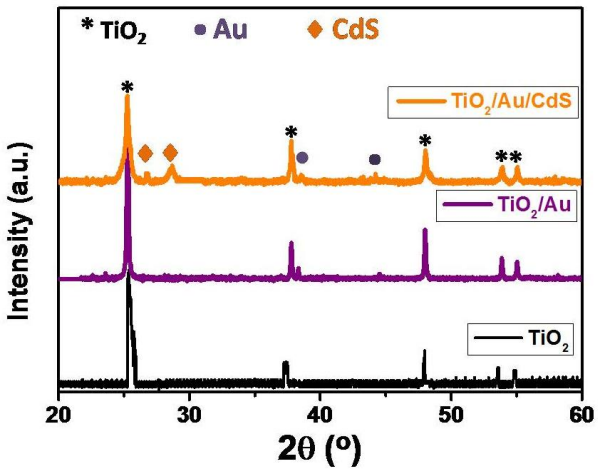

Fig. 1. XRD patterns TiO_2–NFs, Au/TiO_2 NFs and CdS/Au/TiO_2 NFs structures

The morphologies of the $Ti(OiPr)_4$/PVP composite NFs, TiO_2NFs, Au/TiO_2NFs, and CdS/Au/TiO_2NFs are shown in Figure 2. It is obvious that the $Ti(OiPr)_4$/PVP composite NFs form a fibrous structure with varying fiber diameters (Figure 2a). The electrospun PVP/TiOPr composite nanofibers have a smooth surface with fiber diameters ranging from 200 to 550 nm. The surface morphologies of the electrospun TiO_2 NFs are presented in Figure 2b. It is clear that the diameters of the corresponding TiO_2NFs are smaller than those of $Ti(OiPr)_4$/PVP composite NFs because the PVP is removed during calcination. The diameters of TiO_2 NFs range from 150 to 350 nm. TiO_2 NFs are composed of TiO_2 nanoparticles (inset of Figure 2b), aggregated along the fiber orientation. The particle size is about 30 nm. Moreover, the TiO_2 NFs structure has high porosity, created by two types of pores: nano-pores on the surface of each nanofiber due to the burn-out PVP, and macro-pores formed by the random stacking of the fibers. The high porosity of TiO_2 NFs is very convenient for the deposition of other materials since it increases the material permeability. Figure 2c and its inset show the morphology of the Au/TiO_2 NFs sample. The Au NPs are apparent as white dots, decorating the TiO_2 NFs surface. The average particle diameter is 20 nm. It also shows that the Au NPs uniformly cover the entire TiO_2 NFs, which is due to the highly porous structure of the TiO_2 NFs film. The SEM image of the CdS/Au/TiO_2 NFs is presented in Figure 2d. It can be seen that the surface of the TiO_2 NFs are uniformly covered bya CdS layer. The inset in Figure 2d shows a higher magnification of the corresponding image. The particle size of CdS ranges from 10 to 20 nm. This is relatively consistent with the result of XRD.

pISSN 1859-1388
eISSN 2615-9678

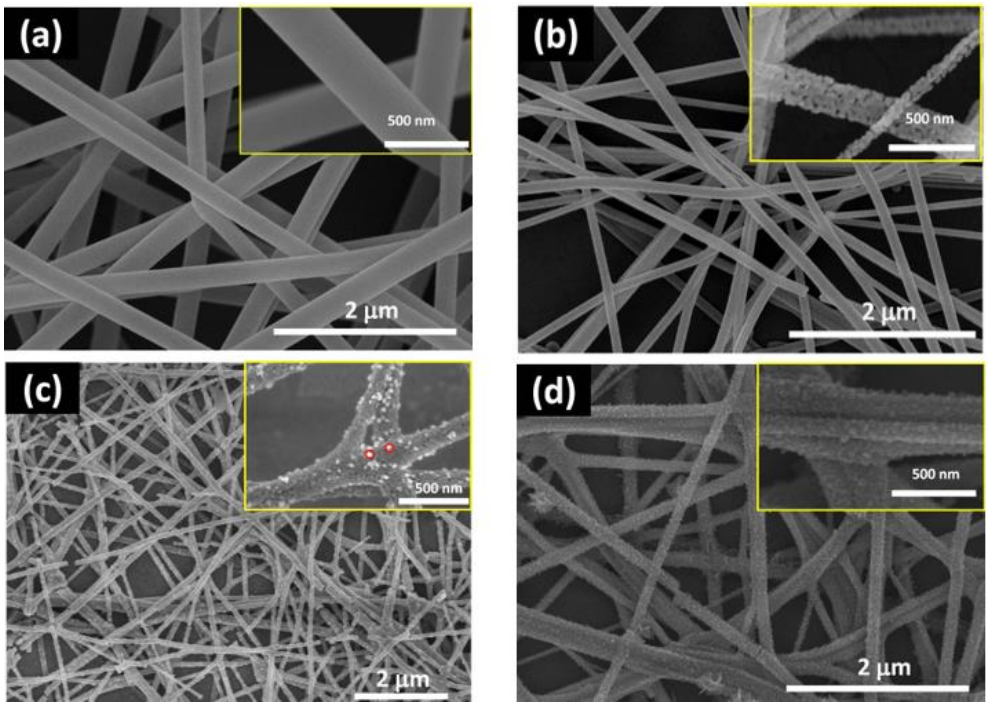

Fig. 2. FE–SEM images of the $Ti(OiPr)_4$/PVP composite NFs (a), TiO_2 NFs (b), Au/TiO_2 NFs (c), and CdS/Au/TiO_2 NFs (d). The insets are enlarged SEM images

The detailed CdS/Au/TiO_2 sandwich structure in the sample was investigated through TEM magnification. As shown in Figure 3a, Au nanoparticles spread on the TiO_2 nanofibers. Although the thickness is about 15 nm, the CdS shell is obviously observed and evenly coated around the Au/TiO_2 NFs. To prove the coexistence of CdS, Au, and TiO_2, the EDX spectra were used to analyze the CdS/Au/TiO_2 sample. Figure 3b shows multiple peaks corresponding to Cd, S, Au, O, and Ti (the peaks for Ca, Na, Si, Mg may belong to the glass substrate). These results are proof of the successful synthesis of the CdS/Au/TiO_2 sandwich structure.

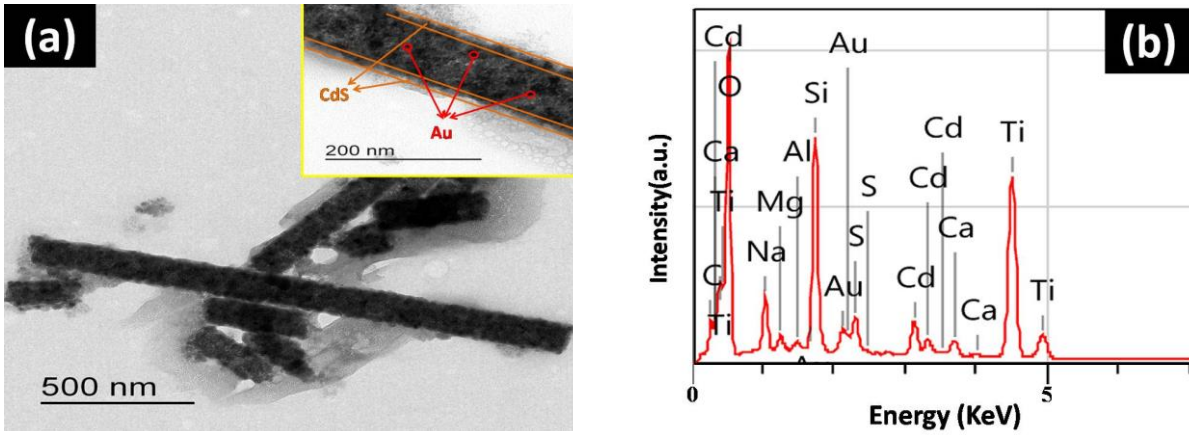

Fig. 3. TEM (a) and EDX (b) of CdS/Au/TiO_2 NFs sample

The optical properties of the samples were analysed by using diffuse reflectance absorption spectra. As shown in Figure 4, all samples can absorb ultraviolet light with wavelengths smaller than 380 nm due to the anatase phase of TiO_2. However, the Au/TiO_2 NFs and CdS/Au/TiO_2 NFs exhibit an absorption peak from 490 to 570 nm in the visible light region due to the SPR effect of Au nanoparticles. The CdS/Au/TiO_2NFs also have another absorption edge due to CdS at 480 nm. This is in agreement with the previous reports [12, 14]. These results are consistent with those from the SEM study. The visible light absorption of CdS/AuTiO_2 NFs films is expected to pave the way for their application in practical water splitting as well as solving the environmental issues.

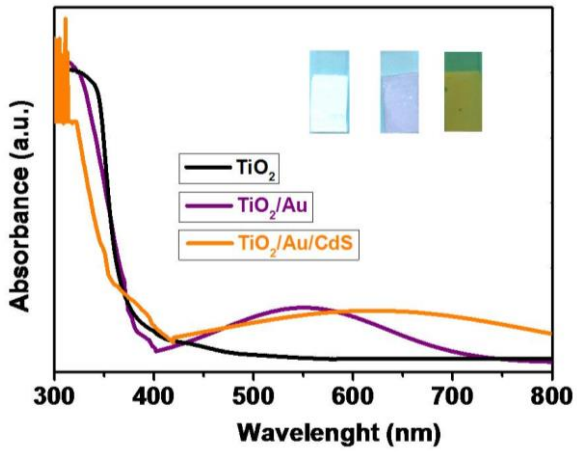

Fig. 4. UV–Vis spectrum TiO_2NFs, Au/TiO_2NFs, and CdS/Au/TiO_2NFs structures

To investigate the photo-electrochemical properties of the prepared samples, photocurrent density and the corresponding photoconversion efficiency for Au/TiO_2 NFs, CdS/TiO_2 NFs, Au/CdS/TiO_2, and CdS/Au/TiO_2 NFs photoelectrodes were measured. Figure 5a shows the dependence of the applied bias potential on the magnitude of photocurrent. Under Xenon lamp illumination, the anodic photocurrent increases with the bias potential and reaches saturation at 0.5 V for all samples. The photocurrent density of CdS/Au/TiO_2, Au/CdS/TiO_2, and CdS/TiO_2 electrodes increases significantly with the applied potential, while the photocurrent density of Au/TiO_2 electrode increases slowly, and the photocurrent density of TiO_2 NFs is very small, and it can be ignored in this case. In addition, the addition of CdS to the Au/TiO_2 electrode can broaden its absorption in the visible range, capture more photons, and thus improving the photoactivity. Accordingly, Figure 5b shows the photoconversion efficiency whose value is in the followingtrend: Au/TiO_2 NFs < CdS/TiO_2 NFs < Au/CdS/TiO_2 < CdS/Au/TiO_2 NFs. The photoconversion efficiency reaches amaximum value of about 4.1% at a corresponding photocurrent density of 4.3 mA·cm^{-2} and V_{bias} = 0.25 V for the CdS/Au/TiO_2 NFs photoanode. These results are comparable with or even superior to those of previous CdS/Au/TiO_2 (or Au/CdS/TiO_2) nanostructure reports [12, 10].

To further evaluate the performance of the prepared-sample-based photoanodes in related energy devices, the photocurrent of CdS/TiO_2 NFs, Au/CdS/TiO_2, and CdS/Au/TiO_2 samples was measured under chopped light illumination at 0 V *vs*. Ag/AgCl. The photoresponse changes dramatically under Xenon illumination. Similarly, the photocurrent returns quickly to the steady-state under dark conditions (Figure 5c). It can be seen that the photocurrent has a small change after 80 s. These results demonstrate that the photoelectrode exhibits less electrochemical corrosion during electrolysis.

To evaluate the effect of the Au NPs SPR, the photo-current density of the CdS/TiO_2 NFs, Au/CdS/TiO_2NFs, and CdS/Au/TiO_2NFs samples under green light illumination from a LED (5074 PLCC6, 0.5 W– 540 nm) are compared in Figure 5d. Almost no photo-current from CdS/TiO_2 photoelectrode is observed in this light region

pISSN 1859-1388
eISSN 2615-9678

because the bandgap of TiO_2 and CdS is larger than the excitation photon energy. In contrast, the photo-current of the Au/CdS/TiO_2 NFs and CdS/Au/TiO_2 NFs photoelectrodes further increases with bias potential under green light illumination. This photoelectrochemical behavior is most likely due to the SPR effect of the Au NPs. Therefore, we can conclude that the introduction of Au NPs to the CdS/TiO_2 NFs increases the light absorption and facilitates the charge transfer at the electrode/electrolyte interface, leading to a significant enhancement of PEC performance. Moreover, the photocurrent density of the CdS/Au/TiO_2NFs is higher than that of the Au/CdS/TiO_2 sample. The reason for this would be discussed in the next section.

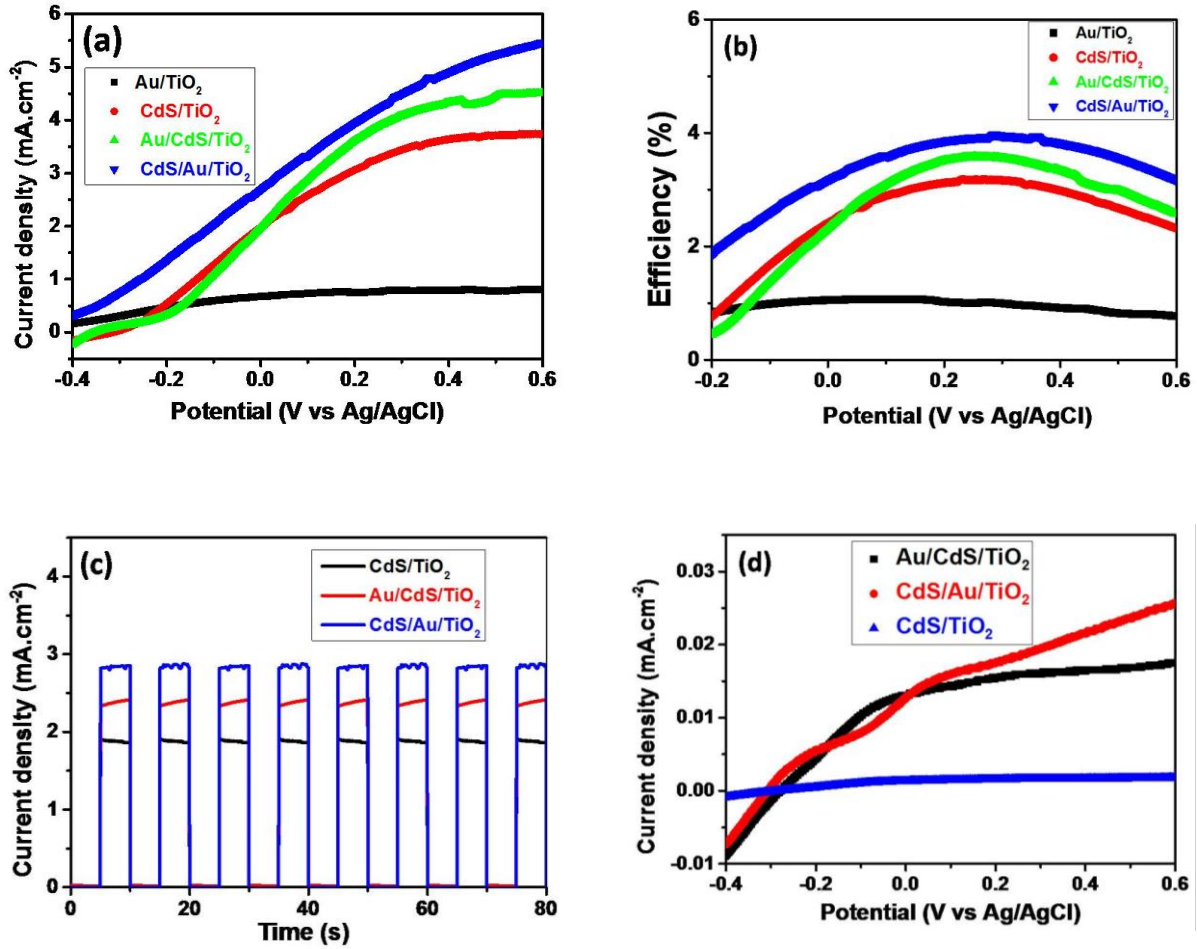

Fig. 5. (a) Photocurrent density, (b) Corresponding photo-conversion efficiencies of Au/TiO_2 NFs, CdS/TiO_2 NFs, Au/CdS/TiO_2 NFs,and CdSAu/TiO_2 NFs, (c) *I–t* curves of CdS/TiO_2 NFs, Au/CdS/TiO_2NFs, and CdS/Au/TiO_2 NFs at V_{bias} = 0 V vs. Ag/AgCl during ON/OFF cycles within 80 s, (d) *I–V* curves of CdS/TiO_2 NFs, Au/CdS/TiO_2NFs, and CdS/Au/TiO_2 under green light irradiation (λ = 540 nm).

On the basis of these results, we propose an electron transfer mechanism on the CdS/Au/TiO_2 NFs, as depicted in Figure 6. At incident light wavelengths shorter than 525 nm, the LSPR in the Au nanoparticles is not excited. Hence, the photocurrent enhancement is not the result of the SPR of Au nanoparticles. Instead, charge carriers are created in the CdS. The photoelectron carriers transfer from CdS to TiO_2 via the Au nanoparticles (the process is shown with the orange arrow). At wavelengths longer than 525 nm, the energy of the light is insufficient to create carriers in the TiO_2 or CdS hence no charge transfer occurs from CdS to TiO_2. However, the SPR is excited in the Au nanoparticles. As reported previously [15], when the plasmonic Au nanoparticles are in intimate contact with TiO_2, hot electrons are excited and can transfer from the plasmonic metal to the conduction band of TiO_2 as shown with the gray arrow. In this case, the Au nanoparticles act as the plasmonic photosensitizer, increasing photoconversion in the wavelength from 525 to 625 nm. Finally, the electrons transfer to the Pt electrode to reduce water and generate hydrogen.

4 Conclusions

In this study, we successfully synthesized a highly stable composite of CdS/Au/TiO_2 NFs sandwich structure. A simple two-step method was used to combine the electrospinning and photodeposition processes. The CdS/Au/TiO_2-NFs-based photoanode exhibits an excellent photocurrent density of 4.3 mA·cm^{-2} at 0.25 V vs. Ag/AgCl, which is much higher than that of CdS/TiO_2-NFs-based photoanode. We believe that the significant improvement in the photoelectrochemical performance of the CdS/Au/TiO_2NFs is the result of the strong CdS/Au/TiO_2 interfacial contact and the SPR effect of the Au nanoparticles. It is expected that this photoanode has promising capacity inenergy storage and conversion applications.

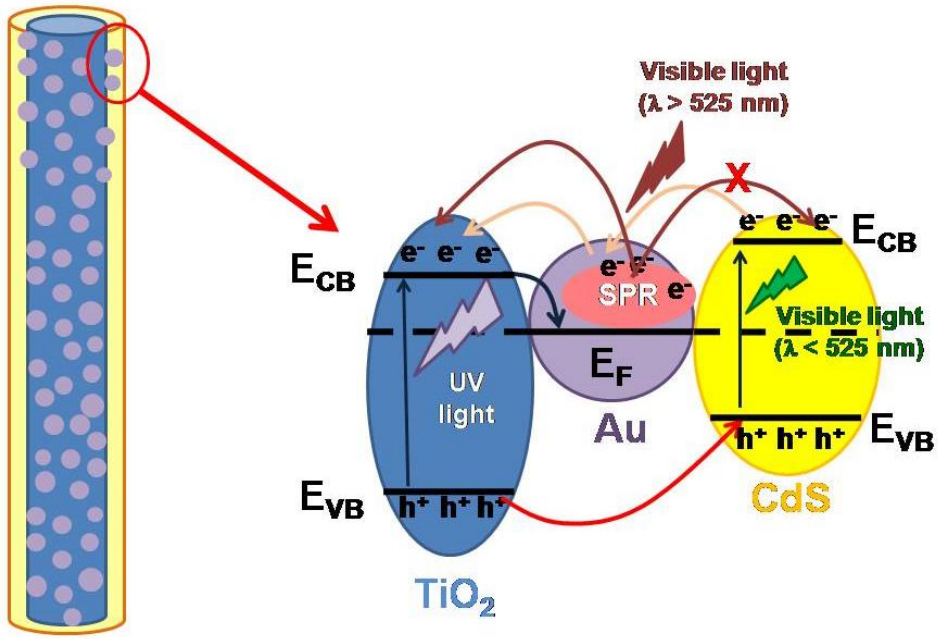

Fig. 6. Charge transfer mechanism CdS/Au/TiO_2 NFs sandwich structure under visible and UV light

pISSN 1859-1388
eISSN 2615-9678

References

1. Khan SUM. Efficient Photochemical Water Splitting by a Chemically Modified n-TiO_2. Science. 2002; 297(5590):2243-2245.
2. Hoang S, Guo S, Hahn NT, Bard AJ, Mullins CB. Visible Light Driven Photoelectrochemical Water Oxidation on Nitrogen-Modified TiO_2 Nanowires. Nano Letters. 2011;12(1):26-32.
3. Sui R, Rizkalla AS, Charpentier PA. Formation of Titania Nanofibers: A Direct Sol–Gel Route in Supercritical CO_2. Langmuir. 2005;21(14):6150-6153.
4. Caratão B, Carneiro E, Sá P, Almeida B, Carvalho S. Properties of Electrospun TiO_2 Nanofibers. Journal of Nanotechnology. 2014;2014:1-5.
5. Chang C, Lee H, Chen C, Wu Y, Hsu Y, Chang Y, et al. A novel rotating electrochemically anodizing process to fabricate titanium oxide surface nanostructures enhancing the bioactivity of osteoblastic cells. Journal of Biomedical Materials Research Part A. 2012;100A(7):1687-1695.
6. Wang H, Liu Y, Zhong M, Xu H, Huang H, Shen H. In situ controlled synthesis of various TiO_2 nanostructured materials via a facile hydrothermal route. Journal of Nanoparticle Research. 2010;13(5):1855-1863.
7. Biernat K, Malinowski A, Malwwina G. The Possibility of Future Biofuels Production Using Waste Carbon Dioxide and Solar Energy. In: Zhen F, editors. Biofuels – Economy, Environment and Sustainability. London (UK): IntechOpen Limited; 2013. p. 123-172.
8. Dholam R, Patel N, Adami M, Miotello A. Hydrogen production by photocatalytic water-splitting using Cr- or Fe-doped TiO_2 composite thin films photocatalyst. International Journal of Hydrogen Energy. 2009;34(13): 5337-5346.
9. Luo J, Ma L, He T, Ng CF, Wang S, Sun H, Fan HJ. TiO_2/(CdS, CdSe, CdSeS) Nanorod Heterostructures and Photoelectrochemical Properties. The Journal of Physical Chemistry C. 2012;116(22):11956-11963.
10. Li J, Cushing SK, Zheng P, Senty T, Meng F, Bristow AD, Manivannan A, Wu N. Solar Hydrogen Generation by a CdS-Au-TiO_2 Sandwich Nanorod Array Enhanced with Au Nanoparticle as Electron Relay and Plasmonic Photosensitizer. Journal of the American Chemical Society. 2014;136(23):8438-8449.
11. Wang H, You T, Shi W, Li J, Guo L. Au/TiO_2/Au as a Plasmonic Coupling Photocatalyst. The Journal of Physical Chemistry C. 2012;116(10):6490-6494.
12. Fang J, Xu L, Zhang Z, Yuan Y, Cao S, Wang Z, et al. Au@TiO_2–CdS Ternary Nanostructures for Efficient Visible-Light-Driven Hydrogen Generation. ACS Applied Materials & Interfaces. 2013;5(16):8088-8092
13. Xu F, Mei J, Zheng M, Bai D, Wu D, Gao Z, et al. Au nanoparticles modified branched TiO_2 nanorod array arranged with ultrathin nanorods for enhanced photoelectrochemical water splitting. Journal of Alloys and Compounds. 2017;693:1124-1132.
14. Song K, Wang X, Xiang Q, Xu J. Weakened negative effect of Au/TiO_2 photocatalytic activity by CdS quantum dots deposited under UV-vis light illumination at different intensity ratios. Physical Chemistry Chemical Physics. 2016;18(42):29131-29138.
15. Su F, Wang T, Lv R, Zhang J, Zhang P, Lu J, et al. Dendritic Au/TiO_2 nanorod arrays for visible-light driven photoelectrochemical water splitting. Nanoscale. 2013;5(19):9001.